ISSN 1674-1056
http://cpb.iphy.ac.cn
http://iopscience.iop.org/cpb
中国物理 B
Chinese Physics
中国物理 Chinese Physics B

Transport of velocity alignment particles in random obstacles

Wei-jing Zhu(朱薇静), Xiao-qun Huang(黄小群), Bao-quan Ai(艾保全)
Citation: Chin. Phys. B . 2018, 27(8): 080504. **doi:** 10.1088/1674-1056/27/8/080504

Journal homepage: http://cpb.iphy.ac.cn; http://iopscience.iop.org/cpb

What follows is a list of articles you may be interested in

Current transport and mass separation for an asymmetric fluctuation system with correlated noises

Jie Wang(王杰), Li-Juan Ning(宁丽娟)
Chin. Phys. B . 2018, 27(1): 010501. **doi:** 10.1088/1674-1056/27/1/010501

An image encryption scheme based on three-dimensional Brownian motion and chaotic system

Xiu-Li Chai(柴秀丽), Zhi-Hua Gan(甘志华), Ke Yuan(袁科), Yang Lu(路杨), Yi-Ran Chen(陈怡然)
Chin. Phys. B . 2017, 26(2): 020504. **doi:** 10.1088/1674-1056/26/2/020504

Current and efficiency optimization under oscillating forces in entropic barriers

Ferhat Nutku, Ekrem Aydiner
Chin. Phys. B . 2016, 25(9): 090501. **doi:** 10.1088/1674-1056/25/9/090501

Current and efficiency of Brownian particles under oscillating forces in entropic barriers

Ferhat Nutku, Ekrem Aydıner
Chin. Phys. B . 2015, 24(4): 040501. **doi:** 10.1088/1674-1056/24/4/040501

Transport of velocity alignment particles in random obstacles*

Wei-jing Zhu(朱薇静)[1], Xiao-qun Huang(黄小群)[2], and Bao-quan Ai(艾保全)[1,†]

[1] Guangdong Provincial Key Laboratory of Quantum Engineering and Quantum Materials, School of Physics and Telecommunication Engineering, South China Normal University, Guangzhou 510006, China

[2] Basic Teaching Department, Neusoft Institute Guangdong, Foshan 528000, China

(Received 20 April 2018; revised manuscript received 4 June 2018; published online 25 July 2018)

We numerically investigate the trapping behaviors of aligning particles in two-dimensional (2D) random obstacles system. Under the circumstances of the effective diffusion rate and the average velocity tend to zero, particles are in trapped state. In this paper, we examine how the system parameters affect the trapping behaviors. At the large self-propelled speed, the ability of nematic particles escape from trapping state is enhancing rapidly, in the meanwhile the polar and free particles are still in trapped state. For the small rotation diffusion coefficient, the polar particles circle around (like vortices) the obstacles and here particles are in trapped state. Interestingly, only the partial nematic particles are trapped in the confined direction and additional particles remain flowing. In the free case, the disorder particle–particle collisions impede the motion in each other's directions, leading the free particles to be trapped. At the large rotation diffusion coefficient, the ordered motion of aligning particles disappear, particles fill the sample evenly and are self-trapped around obstacles. As the particles approach the trapping density due to the crowding effect the particles become so dense that they impede each other's motion. With the increasing number of obstacles, the trajectories of particles are blocked by obstacles, which obstruct the movement of particles. It is worth noting that when the number of the obstacles are large enough, once the particles are trapped, the system is permanently absorbed into a trapped state.

Keywords: Brownian motion, self-propelled particles, stochastic processes

PACS: 05.40.–a, 45.50.–j, 02.50.–r **DOI:** 10.1088/1674-1056/27/8/080504

1. Introduction

Active particles are widespread concerned because their physical properties resemble active microorganisms.[1–11] Active matter systems can be modeled as biological systems.[12] Recent years, fascinating discoveries have been explored active particles with collectively interacting systems.[13–23] Particles are uniform and dense when collections of sterically interacting particles act like a hard disk.

When the particles are active and follow the rules of run-and-tumble dynamics, the system can change phase.[24–34] The transitions of dynamical states and phases address complex environment and have been studied in two-dimensional (2D) or 3D systems.[35–48] The phase transitions of mixed species with different density, including a jammed state, a phase separated state, a mixing phase, and a laning phase, are identified by measuring the average velocity versus the driving force.[35] The transition of a completely clogged state to a flowing state through disordered array of obstacles is achieved when the particles density and activity are increasing, and at large activity the motion of the intermittent state occurs in avalanches.[36] Active particles undergo the jamming and clogging transitions in fixed obstacles,[37] and periodic obstacle arrays.[38] When the system includes particle-particle interaction, the activity induces particles' clustering effects which can occur in driven diffusion.[25,28,31,49] It also shows trapping effects during collective motion. At low activity, particles are easily trapped, however, the ability of particles to escape from the trapped state is enhancing with the increasing activity.[37] The study of a transition to continuum percolation shows that the particles can be trapped above a critical obstacle density.[50] Particles can be in trapped state when they circle around the obstacles.[51] In certain condition, the diffusion of obstacles tends to zero and particles become trapped.[52]

The state of order is one of the interesting phenomena created by nature. The aligning interactions can form the ordered state. Active particles are often used as models to study the physical properties of aligning entities. Active particles with head/tail asymmetry result in polar interactions, however, active particles with head-tail symmetry result in nematic interactions.[53] Birds are keeping polarization of the flock, the paper have proposed a new dynamical equation for the collective movement of polarizing animals.[54] Particles can move with large-scales nematic order in the presence of the hard core repulsive (short range) interactions.[55,56] There has been tremendous increasing interest in the motion of aligning interactions in periodic structure.[57–62] However, these papers do not mainly consider the transitions of dynamical states and

*Project supported by the National Natural Science Foundation of China (Grant Nos. 11575064 and 11175067), the PCSIRT (Grant No. IRT1243), the GDUPS (2016), and the Natural Science Foundation of Guangdong Province, China (Grant No. 2014A030313426).

†Corresponding author. E-mail: aibq@scnu.edu.cn

© 2018 Chinese Physical Society and IOP Publishing Ltd

phases. Here we examine the trapping effects for active particles with aligning interactions in fixed random obstacles.

2. Model and methods

We model active particles moving in a 2D periodic system of size $L \times L$ with $L = 60$ and the system is with periodic boundary conditions in the x direction and hard wall boundary conditions in the y direction. The system contains n_a active particles and n_o randomly obstacles which are the same radius $r/2 = 0.5$, giving the number ratio of 2.75:1. We introduce n_0 obstacles that are identical to the active particles but are permanently fixed in place. The hard core repulsive interactions between particles are $\boldsymbol{F}_{ij} : \boldsymbol{F}_{ij} = k(r - r_{ij})\hat{\boldsymbol{r}}_{ij}$, where k is the spring constant, $r_{ij} = |\boldsymbol{r}_i - \boldsymbol{r}_j|$ and $\hat{\boldsymbol{r}}_{ij} = (\boldsymbol{r}_i - \boldsymbol{r}_j)/r_{ij}$. If $r_{ij} < r$, $\boldsymbol{F}_{ij} = k(r - r_{ij})$. If $r_{ij} > r$, $\boldsymbol{F}_{ij} = 0$. r_{ij} is the distance between particles and $\hat{\boldsymbol{r}}_{ij}$ is the displacement vector. In order to mimic hard particles, we use a large value for the product of spring constant and mobility $\mu k (= 100)$, thus ensuring that particle overlaps decay quickly. The coordinate of particles can be described by $\boldsymbol{r}_i \equiv (x_i, y_i)$. The system is in the overdamped regime, the inertial effects can be neglected. The dynamics of particles can be governed by the Langevin equations

$$\dot{x}_i = v_0 \cos\theta_i + \mu \sum_{i \neq j} \boldsymbol{F}_{ij}^x + \sqrt{2D_0}\xi_{x_i}(t), \tag{1}$$

$$\dot{y}_i = v_0 \sin\theta_i + \mu \sum_{i \neq j} \boldsymbol{F}_{ij}^y + \sqrt{2D_0}\xi_{y_i}(t), \tag{2}$$

$$\dot{\theta}_i = \frac{\alpha}{Z_i(t)} \sum_{|\boldsymbol{r}_j - \boldsymbol{r}_i| < r_0} G_s(\theta_i, \theta_j) + \sqrt{2D_\theta}\xi_{\theta_i}(t), \tag{3}$$

where v_0 is the self-propulsion speed which is oriented at an angle θ with respect to the x and y axes. μ is the mobility. D_0 is the translational diffusion coefficient, the thermal fluctuations are modeled by the Gaussian white noises ξ_{x_i} and ξ_{y_i} with $\langle \xi_i(t) \rangle = 0$, $\langle \xi_i(t)\xi_j(t') \rangle = 2D_0\delta_{ij}\delta(t - t')$. D_θ is the rotational diffusion coefficient, the orientational fluctuation is modeled by the Gaussian white noise ξ_{θ_i} with $\langle \xi_{\theta_i}(t) \rangle = 0$, $\langle \xi_{\theta_i}(t)\xi_{\theta_i}(t') \rangle = 2D_\theta\delta(t - t')$. The Gaussian white noises terms in Eqs. (1)–(3) have been seen to be independent. Strictly speaking, D_0 and D_θ may be correlated in statistics.[63] α is the aligning intensity. Z_i[58,59,64,65] is the current number of neighbors of particle i within r_0. To quantify the aligning interaction, we consider the parameter G_s, $G_s(\theta_j, \theta_i) = s\sin(\theta_j - \theta_i) + (1 - s)\sin 2(\theta_j - \theta_i)$. s denotes the relative weight of the polar interactions. Polar interactions with head/tail asymmetric cause particles to move to parallel direction, while nematic interactions with head-tail symmetry result in the motion of antiparallel direction. For the polar alignment interactions, $s = 1.0$ and $\alpha = 1.0$; For the nematic alignment interactions, $s = 0.0$ and $\alpha = 1.0$; For the free alignment interactions, $s = 1.0$ and $\alpha = 0.0$.

Before the statistical simulation, we can rewrite Eqs. (1)–(3) in the dimensionless forms, giving the characteristic length scale $\hat{x} = x/r$, $\hat{y} = y/r$ and the time scale $\hat{t} = \mu k t$.

$$\hat{\dot{x}}_i = \hat{v}_0 \cos\theta_i + \sum_{i \neq j} \hat{\boldsymbol{F}}_{ij}^x + \sqrt{2\hat{D}_0}\hat{\xi}_{x_i}(\hat{t}), \tag{4}$$

$$\hat{\dot{y}}_i = \hat{v}_0 \sin\theta_i + \sum_{i \neq j} \hat{\boldsymbol{F}}_{ij}^y + \sqrt{2\hat{D}_0}\hat{\xi}_{y_i}(\hat{t}), \tag{5}$$

$$\dot{\theta}_i = \frac{\hat{\alpha}}{Z_i(\hat{t})} \sum_{|\hat{\boldsymbol{r}}_j - \hat{\boldsymbol{r}}_i| < \hat{r}_0} G_s(\theta_j, \theta_i) + \sqrt{2\hat{D}_\theta}\hat{\xi}_{\theta_i}(\hat{t}), \tag{6}$$

where $\hat{v}_0 = v_0/\mu k r$, $\hat{\boldsymbol{F}}_{ij}^x = \boldsymbol{F}_{ij}^x/kr$, $\hat{\boldsymbol{F}}_{ij}^y = \boldsymbol{F}_{ij}^y/kr$, $\hat{D}_0 = D_0/\mu k r^2$, $\hat{D}_\theta = D_\theta/\mu k$, $\hat{\alpha} = \alpha/\mu k$, $\hat{r}_0 = r_0/r$, $\hat{L} = L/r$. From now on, we will only use the dimensionless variables and omit the hat for all quantities appearing in the above equations.

To quantify the trapping transition, we introduce the average velocity in the x direction, $V_x = v/v_0$ where $v = \lim_{t\to\infty} \langle x(t) - x(0) \rangle / t$. Meanwhile, We define the effective diffusion rate in the x direction, $D_x = D_e/D_f$ where $D_e = \lim_{t\to\infty} \langle x(t) - \langle x(t) \rangle \rangle^2 / 2t$. D_f is the free diffusion coefficient, $D_f = D_0 + v_0^2/2D_\theta$.

To ensure that the system reached a steady state, we have chosen the integration steps time Δt to be smaller than 10^{-3} and run all the simulation for more than 10^6.

3. Results and discussion

In Figs. 1(a) and 1(b) we plot D_x and V_x versus v_0 for the polar, nematic and free aligning interactions. At the small self-propelled speed of $v_0 \to 0$, particles' behaviors fall in the passive particles limit and the aligning interactions become less important thus the dynamic behaviors are the same for three cases; here the particles have no dynamic fluctuations and become trapped. As v_0 increases, for the polar case D_x and V_x pass through their maximum value. It indicates that the particles can move easily through the system, resulting in the amount of trapping being significantly reduced. When the v_0 increases to higher value, $D_x \to 0$ and $V_x \to 0$. For the nematic case, the particles are trapped completely at $v_0 < 3$. As v_0 increases, the ability of particles moves away from the trapped state is enhanced. In the free case, the disordered particles have no obvious dynamics fluctuations with the variety of v_0.

In Fig. 2(a) we show the final V_x=0 and D_x=0 configuration from Fig. 1(a) of the polar case, which reaches a trapped state. Polar interactions with head/tail asymmetric lead particles to move to parallel direction. As we can see from

the Fig. 2(a), almost of all particles which with parallel order move toward to the upper edge of sample, at the same time they are gather in the confined direction where particles are trapped. Figure 2(b) shows the final configuration from Fig. 1(a) of the nematic case. Here particles are divided into two parts. Based on the nematic particles with head-tail symmetry, they can move to anti-parallel direction. A portion of the particles are trapped in the y direction, while additional particles have directional motion in the negative x direction. This configuration provides a good explanation for the increasing ability of nematic particles to escape the trapped state.

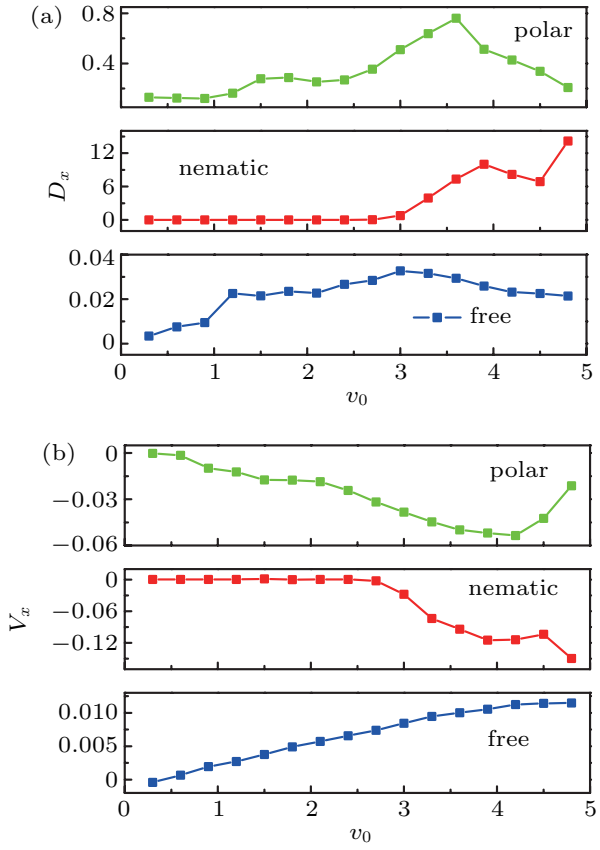


Fig. 1. (color online) (a) Effective diffusion rate D_x as a function of the self-propulsion speed v_0 for polar, nematic and free aligning interactions. (b) Average velocity V_x versus the self-propulsion speed v_0 for three cases. The other parameters are: $D_\theta = 0.1$, $D_0 = 0.01$, $n_o = 80$, and $n_a = 220$.

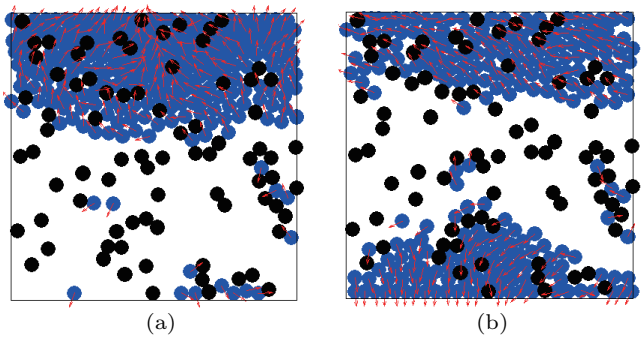


Fig. 2. (color online) The dynamic configuration of the particles (blue circles) and random obstacles (black circles) from Figs. 1(a) and 1(b). (a) Final trapped configuration of the polar cases. (b) Final trapped configuration of the nematic case.

In Fig. 3(a) we plot D_x and V_x versus D_θ with polar, nematic and free aligning interactions. The trend of three cases emerges from data. At low D_θ, D_x and V_x tend to zero. As D_θ increases, D_x and V_x pass through the maximum value after decreasing. The decreasing of D_x and V_x indicate that particles become trapped around obstacles.

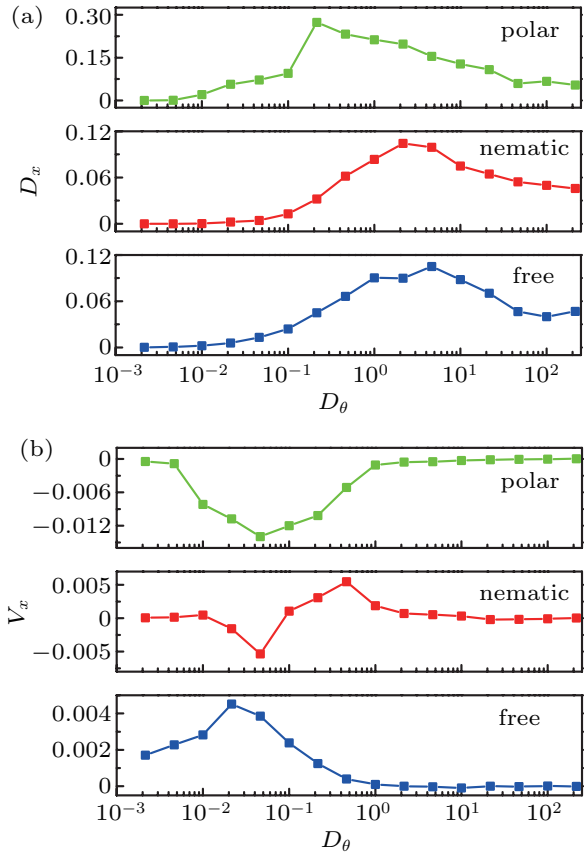


Fig. 3. (color online) (a) Effective diffusion rate D_x versus the rotational diffusion coefficient D_θ for polar, nematic and free aligning interactions. (b) Dependence of the average velocity V_x on the rotational diffusion coefficient D_θ. The other parameters are: $v_0 = 1.0$, $D_0 = 0.01$, $n_o = 80$, and $n_a = 220$.

Figures 4(a)–4(c) show the configuration of the polar, nematic and free aligning interactions from Figs. 3(a) and 3(b) at low D_θ. In Fig. 4(a) the polar particles with head/tail asymmetric circle around the obstacles (like vortices) and here particles are in trapped state.[51] In Fig. 4(b), a portion of the nematic particles (the particles of moving in the x direction) with head-tail symmetry move orderly to anti-parallel directions which can offset the dynamics fluctuation. Additional nematic particles (the particles of moving in the y direction) are trapped in the confined direction. In Fig. 4(c), the free particles gather in the corner of sample. It indicates that disordered particle-particle collisions impede the motion in each other's directions, resulting in particles being trapped in the corner. At high D_θ, the final configuration of three cases is the same (see Fig. 4(d)). The ordered motion of aligning particles disappears, particles fill the space evenly. Since high D_θ can break the directional motion and eliminate the order of

aligning particles, leading particles to be self-trapped around obstacles. The particles can be trapping evenly around the obstacles, meaning that the "deepest" trapping are effectively inactivated.

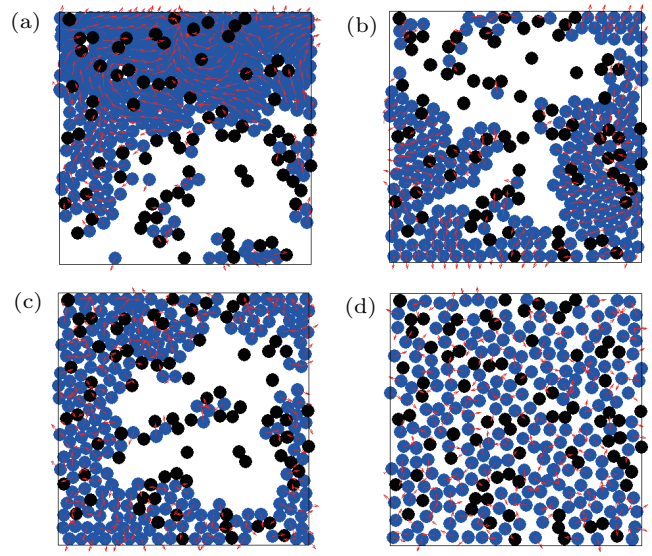


Fig. 4. (color online) The dynamic configuration of the particles (blue circles) and random obstacles (black circles) from Figs. 3(a) and 3(b). (a) Final configuration of the polar case at low D_θ. (b) Final configuration of the nematic case at low D_θ. (c) Final configuration of the free case at low D_θ. (d) Final configuration of three cases at high D_θ.

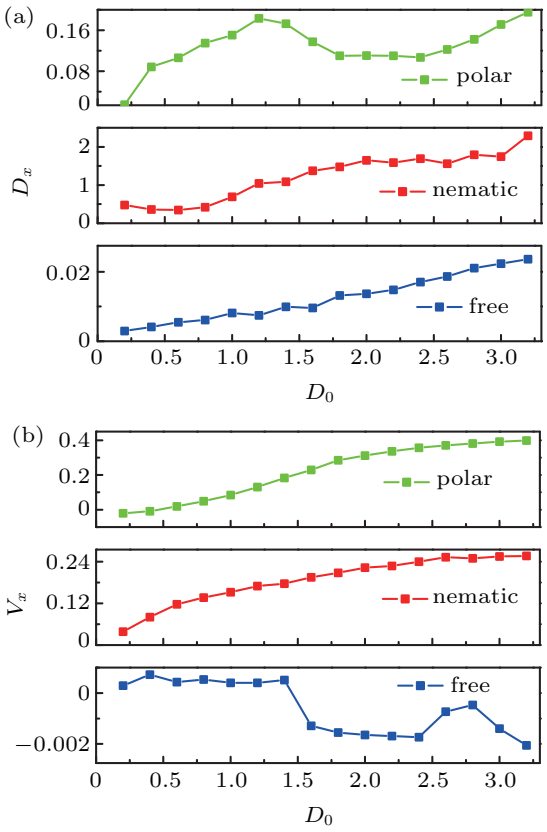


Fig. 5. (color online) (a) D_x versus D_0 for polar, nematic and free cases. (b) V_x versus D_0 for three cases. The other parameters are: $v_0 = 1.0$, $D_\theta = 0.1$, $n_o = 80$, and $n_a = 220$.

In Figs. 5(a) and 5(b) we show the D_x and V_x as a function of the D_0 for polar, nematic, and free cases. At small D_0, D_x and V_x tend to zero. At large D_0, D_x and V_x of the aligning particles are larger and finite. That is D_0 can activate particles motion, particles could "jump" from trapping state and the ability of particles to escape from the trapping state continues to enhance. Compared with aligning particles, the free particles have no obvious change with the variety of D_0.

The plot of D_x and V_x versus n_a in Figs. 6(a) and 6(b) for three cases. For the free cases, V_x and D_x from finite value drop to zero. For polar and nematic cases, D_x and V_x increase with increasing n_a and then decrease for higher n_a. As the particles approach the trapping density, due to the crowding effect, the active particles become so dense that they impede each other's motion.

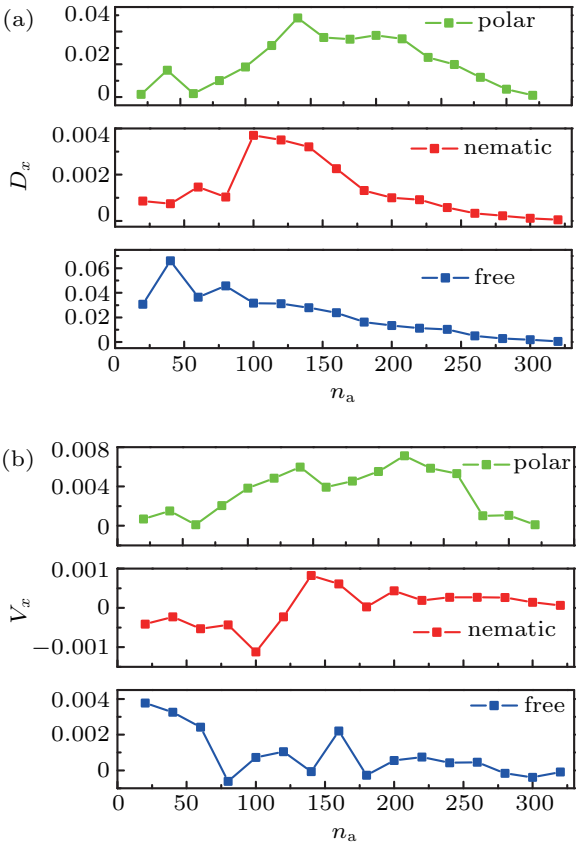


Fig. 6. (color online) (a) Effective diffusion rate D_x as a function of the number of active particles n_a for polar, nematic and free cases. (b) Average velocity V_x as a function of the number of active particles n_a for three cases. The other parameters are: $v_0 = 1.0$, $D_0 = 0.01$, $D_\theta = 0.1$, and $n_o = 80$.

The influence of the number of obstacles n_o on D_x and V_x for three cases appears in Figs. 7(a) and 7(b). At small enough n_o of $n_o \to 0$ (not shown in figure), almost all particles are freely flowing in the obstacle-free system. In the limit of $n_o \to 130$, $D_x = 0$ and $V_x = 0$. Here the motion of the particles are eliminated. Owing to with the increasing number of obstacles, the trajectories of particles are blocked by obstacles which obstruct the movement of particles. It is worth noting that when the number of the obstacles are large enough, once the particles are trapped, the system is permanently absorbed into a trapped state.

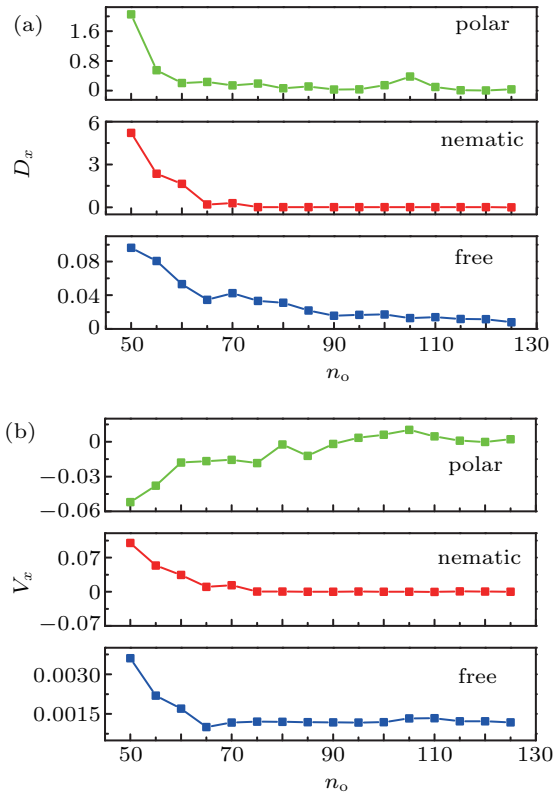


Fig. 7. (color online) (a) D_x versus n_o for polar, nematic and free cases. (b) V_x versus n_o for three cases. The other parameters are: $v_0 = 1.0$, $D_0 = 0.01$, $D_\theta = 0.1$, and $n_a = 220$.

4. Conclusion

We have examined how the aligning particles are trapped in a two-dimensional random obstacles system. Under the circumstances of the effective diffusion rate and the average velocity tend to zero, particles are in trapped state. It is known that passive particles are easily trapped without dynamics fluctuations. At the large self-propelled speed, the polar particles are trapped in the upper edge of sample. However, the ability of the nematic particles escape from the trapped state is enhanced as the self-propelled speed increases. Additionally, for the free particles, compared with aligning particles these disordered particles have no obvious dynamics fluctuations with the variety of the self-propelled speed. At the small rotation diffusion coefficient, the polar particles circle around (like vortices) the obstacles and here particles are in trapped state. And the partial nematic particles are trapped in the confined direction. In the free case, the disordered particle–particle collisions impede the motion in each other's directions. At the large rotation diffusion coefficient, the three cases have the same configuration. The ordered motion of aligning particles disappear, particles fill the space evenly and are self-trapped around obstacles. We found that only the nematic particles increase the ability escape the trapped state with the increasing of the translational diffusion coefficient. When the number of particles increase, as the particles approach the trapping density due to the crowding effect the active particles become so dense that they impede each other's motion. We also found that with the increasing number of obstacles, the trajectories of particles are blocked by obstacles which obstruct the movement of particles. It is worth noting that when the number of the obstacles are large enough, once the particles are trapped, the system is permanently absorbed into a trapped state. Above results may be applied to particles separation or mixing.

References

[1] Paxton W F, Kistler K C, Olmeda C C, Sen A, Angelo S K St, Cao Y, Mallouk T E, Lammert P E and Crespi V H 2004 *J. Am. Chem. Soc.* **126** 41
[2] Bechinger C, Leonardo R D, Löwen H, Reichhardt C, Volpe G and Volpe G 2016 *Rev. Mod. Phys.* **88** 045006
[3] Dreyfus R, Baudry J, Roper M L, Fermigier M, Stone M L and Bibette J 2005 *Nature* **437** 862
[4] Howse J R, Jones R A L, Ryan A J, Gough T, Vafabakhsh R and Golestanian R 2007 *Phys. Rev. Lett.* **99** 048102
[5] Palacci J, Cottin-Bizonne C, Ybert C and Bocquet L 2010 *Phys. Rev. Lett.* **105** 088304
[6] Jiang H R, Yoshinaga N and Sano M 2010 *Phys. Rev. Lett.* **105** 268302
[7] Buttinoni I, Volpe G, Kümmel F, Volpe G and Bechinger C 2012 *J. Phys.: Condens. Matter* **24** 284129
[8] Romanczuk P, Bär M, Ebeling W, Lindner B and Schimansky-Geier L 2012 *Eur. Phys. J. Special Topics* **202** 1
[9] Zöttl A and Stark H 2012 *Phys. Rev. Lett.* **108** 218104
[10] Cates M 2012 *Rep. Prog. Phys.* **75** 042601
[11] Elgeti J, Winkler R G and Gompper G 2015 *Rep. Prog. Phys.* **78** 056601
[12] Feng Y L, Dong J M and Tang X L 2016 *Chin. Phys. Lett.* **33** 108701
[13] Bhattacharya S and Higgins M J 1993 *Phys. Rev. Lett.* **70** 2617
[14] Koshelev A E and Vinokur V M 1994 *Phys. Rev. Lett.* **73** 3580
[15] Olson C J, Reichhardt C and Nori F 1998 *Phys. Rev. Lett.* **81** 3757
[16] Williams F I B, Wright P A, Clark R G, Andrei E Y, Deville G, Glattli D C, Probst O, Etienne B, Dorin C, Foxon C T and Harris J J 1991 *Phys. Rev. Lett.* **66** 3285
[17] Pertsinidis A and Ling X S 2008 *Phys. Rev. Lett.* **100** 028303
[18] Tierno P 2012 *Phys. Rev. Lett.* **109** 198304
[19] Bohlein T, Mikhael J and Bechinger C 2012 *Nat. Mater.* **11** 126
[20] Reichhardt C and Reichhardt C J O 2012 *Phys. Rev. E* **85** 051401
[21] Mcdermott D, Amelang J, Reichhardt C J O and Reichhardt C 2013 *Phys. Rev. E* **88** 062301
[22] Braun O M, Dauxois T, Paliy M V and Peyrard M 1997 *Phys. Rev. Lett.* **78** 1295
[23] Vanossi A, Manini N, Urbakh M, Zapperi S and Tosatti E 2013 *Rev. Mod. Phys.* **85** 529
[24] Tian W D, Gu Y, Guo Y K and Chen K 2017 *Chin. Phys. B* **26** 100502
[25] Palacci J, Sacanna S, Steinberg A P, Pine D J and Chaikin P M 2013 *Science* **339** 936
[26] Bialké J, Speck T and Löwen H 2012 *Phys. Rev. Lett.* **108** 168301
[27] Henkes S, Fily Y and Marchetti M C 2011 *Phys. Rev. E* **84** 040301
[28] Fily Y and Marchetti M C 2012 *Phys. Rev. Lett.* **108** 235702
[29] Cates M E and Tailleur J 2013 *Europhys. Lett.* **101** 20010
[30] Theurkauff I, Cottin-Bizonne C, Palacci J, Ybert C and Bocquet L 2012 *Phys. Rev. Lett.* **108** 268303
[31] Redner G S, Hagan M F and Baskaran A 2013 *Phys. Rev. Lett.* **110** 055701
[32] Buttinoni I, Bialké J, Kümmel F, Löwen H, Bechinger C and Speck T 2013 *Phys. Rev. Lett.* **110** 238301
[33] Stenhammar J, Tiribocchi A, Allen R J, Marenduzzo D and Cates M E 2013 *Phys. Rev. Lett.* **111** 145702
[34] Mognetti B M, Saric A, Angioletti-Uberti S, Cacciuto A, Valeriani C and Frenkel D 2013 *Phys. Rev. Lett.* **111** 245702
[35] Reichhardt C and Reichhardt C J O 2017 *Soft Matter* **14** 4
[36] Reichhardt C and Reichhardt C J O 2017 *New J. Phys.* **20** 2
[37] Reichhardt C and Reichhardt C J O 2014 *Phys. Rev. E* **90** 012701
[38] Nguyen H T, Reichhardt C and Reichhardt C J O 2017 *Phys. Rev. E* **95** 030902

[39] Reichhardt C and Reichhardt C J O 2018 *J. Phys. Condens. Matter* **30** 015404
[40] O'Hern C S, Silbert L E, Liu A J and Nagel S R 2003 *Phys. Rev. E* **68** 011306
[41] Drocco J A, Hastings M B, Reichhardt C J O and Reichhardt C 2005 *Phys. Rev. Lett.* **95** 088001
[42] Reichhardt C and Reichhardt C J O 2014 *Soft Matter* **10** 2932
[43] To K, Lai P -Y and Pak H K 2001 *Phys. Rev. Lett.* **86** 71
[44] Thomas C C and Durian D J 2013 *Phys. Rev. E* **87** 052201
[45] Garcimartín A, Pastor J M, Ferrer L M, Ramos J J, Martín-Gómez C and Zuriguel I 2015 *Phys. Rev. E* **91** 022808
[46] Zuriguel I, Pugnaloni L A, Garcimartín A and Maza D 2003 *Phys. Rev. E* **68** 030301
[47] Morin A, Desreumaux N, Caussin J B and Bartolo D 2017 *Nat. Phys.* **13** 63
[48] Zeitz M, Wolff K and Stark H 2017 *Eur. Phys. J. E* **40** 23
[49] Reichhardt C and Reichhardt C J O 2015 *Phys. Rev. E* **91** 032313
[50] Mertens S and Moore C 2012 *Phys. Rev. E* **86** 061109
[51] Chepizhko O and Peruani F 2013 *Phys. Rev. Lett.* **111** 160604
[52] Reichhardt C and Reichhardt C J O 2014 *Soft Matter* **10** 7502
[53] Baskaran A and Marchetti M C 2012 *Eur. Phys. J. E* **35** 95
[54] Cavagna A, Castello L D, Giardina I, Grigera T, Jelic A, Melillo S, Mora T, Parisi L, Silvestri E, Viale M and Walczak A M 2015 *J. Stat. Phys.* **158** 601
[55] Baskaran A and Marchetti M C 2008 *Phys. Rev. Lett.* **101** 268101
[56] Baskaran A and Marchetti M C 2009 *Proc. Natl. Acad. Sci. USA* **106** 15567
[57] Vicsek T, Czirok A, Ben-Jacob E, Cohen I and Shochet O 1995 *Phys. Rev. Lett.* **75** 1226
[58] Ngo S, Ginelli F and Chaté H 2012 *Phys. Rev. E* **86** 050101
[59] Nagai K H, Sumino Y, Montagne R, Aranson I S and Chaté H 2015 *Phys. Rev. Lett.* **114** 168001
[60] Ginelli F, Peruani F, Bär M and Chaté H 2010 *Phys. Rev. Lett.* **104** 184502
[61] Zhu W J, Li F G and Ai B Q 2017 *Eur. Phys. J. E* **40** 59
[62] Ai B Q, Zhu W J, He Y F and Zhong W R 2017 *J. Stat. Mech.* **2017** 023501
[63] Mijalkov M and Volpe G 2013 *Soft Matter* **9** 6376
[64] Peruani F and Bär M 2013 *New J. Phys.* **15** 065009
[65] Peruani F, Ginelli F, Bär M and Chaté H 2011 *J. Phys.: Conf. Ser.* **297** 012014